Biophysical Chemistry 138 (2008) 29–35

Contents lists available at ScienceDirect

Biophysical Chemistry

journal homepage: http://www.elsevier.com/locate/biophyschem

Self-assembly in aqueous solution of a modified amyloid beta peptide fragment

V. Castelletto [a], I.W. Hamley [a,*], P.J.F. Harris [b]

[a] Department of Chemistry, The University of Reading, Reading RG6 6AD, UK
[b] Centre for Advanced Microscopy, The University of Reading, Reading RG6 6AF, UK

ARTICLE INFO

Article history:
Received 30 July 2008
Received in revised form 22 August 2008
Accepted 22 August 2008
Available online 3 September 2008

Keywords:
Amyloid
Peptide
Fibrils
Self-assembly

ABSTRACT

The self-assembly in films dried from aqueous solutions of a modified amyloid beta peptide fragment is studied. We focus on sequence Aβ(16–20), KLVFF, extended by two alanines at the N-terminus to give AAKLVFF. Self-assembly into twisted ribbon fibrils is observed, as confirmed by transmission electron microscopy (TEM). Dynamic light scattering reveals the semi-flexible nature of the AAKLVFF fibrils, while polarized optical microscopy shows that the peptide fibrils crystallize after an aqueous solution of AAKLVFF is matured over 5 days. The secondary structure of the fibrils is studied by FT-IR, circular dichroism and X-ray diffraction (XRD), which provide evidence for β-sheet structure in the fibril. From high resolution TEM it is concluded that the average width of an AAKLVFF fibril is (63 ± 18) nm, indicating that these fibrils comprise beta-sheets with multiple repeats of the unit cell, determined by XRD to have *b* and *c* dimensions 1.9 and 4.4 nm with an *a* axis 0.96 nm, corresponding to twice the peptide backbone spacing in the antiparallel β-sheet.

1. Introduction

The formation of fibrils by peptides or proteins under appropriate solution conditions is relevant to amyloid diseases such as Alzheimer's [1]. Understanding the process of peptide fibrillisation in terms of peptide structure and intermolecular interactions is therefore of great interest. Fibrils are commonly based on hydrogen-bonded β-sheets, and the precise details of β-strand packing will depend on non-covalent forces including aromatic π −π* stacking interactions, hydrophobic interactions and electrostatic interactions.

We have recently been investigating the self-assembly of peptides based on a core sequence of the amyloid β peptide. The amyloid β peptide is important in Alzheimer's, a so-called amyloid disease and is cleaved in vivo from a larger precursor protein to form fragments with predominantly 40 or 42 residues [1–3]. We have focussed on sequence KLVFF, corresponding to Aβ(16–20). This core sequence of the amyloid β peptide is believed to be critical in the aggregation of Aβ into fibrils, as reviewed elsewhere [1]. We have examined its self-assembly in aqueous solution [4] due to controversy as to whether it forms β-sheet fibrils or not. We find clear evidence from in situ cryo-TEM (transmission electron microscopy) and small-angle X-ray scattering experiments that it does fibrillise and Fourier transform infra-red (FT-IR) spectroscopy and fibre X-ray diffraction confirm β-sheet structure (we discuss in detail the effects of drying during sample preparation) [4]. This sample also forms hydrogels in more concentrated solution [4].

We have prepared variants of KLVFF extended at the N-terminus with additional hydrophobic residues with the aim to investigate the role of hydrophobic and aromatic interactions on peptide self-assembly. In particular, we have examined the fibrillisation of FFKLVFF in methanol (the peptide is too hydrophobic to dissolve in water) and found evidence for β-sheet self-assembly [5]. We propose that this is driven in large part by aromatic interactions between F residues, as confirmed by UV (ultraviolet) and CD (circular dichroism) spectroscopy.

A sample with non-aromatic residues at one terminus, AAKLVFF, was also prepared [6]. This has solubility in both aqueous and non-aqueous solvents. The self-assembly of AAKLVFF in methanol is reported elsewhere [6]. We show that when dissolved in methanol, AAKLVFF self-assembles into nanotubes, which can form a nematic phase at sufficiently high concentration [6]. The present paper presents a comprehensive study on the self-assembly of AAKLVFF in aqueous solution. Our studies reveal that the peptide self-assembles into very well ordered fibrils in films prepared by drying aqueous solutions. The structure of the AAKLVFF fibrils was studied by transmission electron microscopy (TEM) and dynamic light scattering (DLS). Polarized optical microscopy (POM) was used to quantify the ageing behaviour of the fibrils. The secondary structure of the peptide fibrils was studied by FT-IR, circular dichroism (CD and X-ray diffraction (XRD).

2. Experimental

2.1. Materials

AAKLVFF was custom synthesized by C.S. Bio Company (USA) and was used as received, without further purification. Scheme 1 shows

* Corresponding author. Tel.: +44 118 378 6341; fax: +44 118 378 6331.
E-mail address: I.W.Hamley@reading.ac.uk (I.W. Hamley).

0301-4622/$ – see front matter © 2008 Elsevier B.V. All rights reserved.
doi:10.1016/j.bpc.2008.08.007

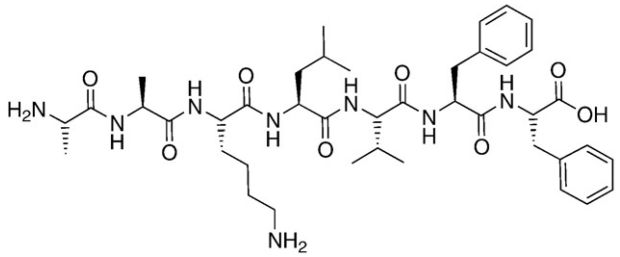

Scheme 1. Molecular structure of AAKLVFF.

the chemical structure of AAKLVFF. Solutions were made using amounts of peptide and Millipore filtered water. The solutions were mixed using a magnetic stirrer for 1 h and left to rest for the following two hours. Experiments were performed within 12 h of sample preparation, with the exception of the POM experiment, which was performed after 5 days of sample preparation (to allow for the ageing of the solution).

2.2. TEM

Experiments were performed using a Philips CM20 transmission electron microscope operated at 80 kV while HR-TEM was done using a JEOL microscope operated at 100 kV. Droplets of the peptide solution (1 wt.% AAKLVFF) was placed on Cu grids coated with a carbon film (Agar Scientific, UK), stained with uranyl acetate (1 wt.%) (Agar Scientific, UK) and dried.

2.3. DLS

Experiments were performed using an ALV CGS-3 system with 5003 multi-digital correlator. The light source was a 20 mW He–Ne laser, linearly polarized, with $\lambda = 633$ nm. Scattering angles in the range $50 \le \theta \le 150°$ were used for all the experiments. Samples containing 0.5 and 1 wt.% AAKLVFF were filtered through 0.20-μm Anotop filters from Whatman into standard 0.5 cm diameter cylindrical glass cells.

DLS experiments measured the intensity correlation function:

$$g^{(2)}(q,t) = \langle I(q,0)I(q,t)\rangle_\tau / \langle I(q,0)\rangle_\tau^2 \quad (1)$$

where $q = [4\pi n \sin(\theta/2)]/\lambda$ is the scattering vector (λ = vacuum wavelength of the radiation and n = refractive index of the medium) and $I(q,t)$ is the intensity scattered by the sample at time t in the course of an experiment of duration τ.

The measured intensity correlation function is related to the field correlation function, $g^{(1)}(q,t)$, by the Siegert relationship [7]:

$$g^{(2)}(q,t) = 1 + A\left[g^{(1)}(q,t)\right]^2 \quad (2)$$

where A is an experimental constant proportional to the ratio between the coherence area and the detector area, which takes the value 0.5 for our experimental setup.

2.4. POM

Images were obtained with an Olympus BX41 polarized microscope by placing the sample between crossed polarizers. Samples were placed between a glass slide and a coverslip before capturing the images with a Canon G2 digital camera.

2.5. Circular dichroism

The CD spectra were recorded on a Chirascan spectropolarimeter (Applied Photophysics, UK). The peptide solution (1 wt.% AAKLVFF) was loaded into a 0.1 mm quartz cell. CD experiments were also performed on a dried film from a 0.5 wt.% AAKLVFF solution, obtained by drying a few drops of the solution on a cover slip. Spectra were obtained from 200 to 260 nm with a 0.5 nm step and 2 s collection time per step at 20 °C, taking five averages. The absorbance A was monitored and the CD data is presented for $A < 2$ at any measured point.

2.6. FT-IR

Spectra were recorded using a Nexus-FT-IR spectrometer equipped with a DTGS detector and a multiple reflection ATR system. Transmission FT-IR measurements were performed using a CaF_2 plate, while grazing angle FT-IR experiments were done using a ZnSe plate. For both transmission and grazing angle configurations, small aliquots of a 1 wt.% AAKLVFF solution were deposited on the corresponding plate and allowed to dry, providing a solid film of dry peptide. Spectra were scanned 64 times and 128 times for transmission and grazing angle geometries respectively, over the range of 4000–400 cm^{-1}.

2.7. XRD

X-ray diffraction was performed on stalks prepared by drying filaments of the peptide. An aqueous solution of the peptide (1 wt.%) was suspended between the ends of wax-coated capillaries and dried. The stalks were mounted (vertically) onto the four axis goniometer of a RAXIS IV++ X-ray diffractometer (Rigaku) equipped with a rotating anode generator. The XRD data was collected using a Saturn 992 CCD camera.

3. Results and discussion

The self-assembled morphology of AAKLVFF in water was studied by TEM and HR-TEM and DLS. The time evolution of fibrillar aggregates was studied by POM. In a second stage, the secondary structure of AAKLVFF fibrils was assessed using CD, FT-IR and XRD. The presentation of our results starts with a discussion of the fibrillar structure, followed by the spectroscopy results on the secondary structure.

3.1. Self-organisation of AAKLVFF

Solutions containing 1 wt.% AAKLVFF were studied by TEM and HR-TEM. Fig. 1a–b shows TEM images for a dried film. It was observed that AAKLVFF fibrils were well defined; with a high polydispersity in length. The TEM image in Fig. 1a reveals that the fibrils are twisted. A detail of this twisting is shown in Fig. 1b which presents an image obtained via HR-TEM. According to the images in Fig. 1a–b, each fibre appears to comprise three (21 ± 6) nm wide protofilaments. The average width of fibrils is (63 ± 18) nm while the pitch of the helically twisted fibrils is very polydisperse, being approximately (770 ± 370) nm. TEM and HR-TEM did not provide a definite value for the fibril length. However, it was possible to determine that 1 wt.% AAKLVFF solutions contain fibrils longer than 5000 nm.

DLS experiments were undertaken in order to evaluate the flexibility of AAKLVFF fibrils in solution. Fig. 2 shows the intensity correlation functions measured at 90° for 1 and 0.5 wt.% AAKLVFF. DLS experiments were initially done on 1 wt.% AAKLVFF samples, but these samples gave evidence not only of fibril formation but also of the onset of gelation. Indeed, the broad peak measured in the intensity correlation function for longer diffusion times indicates non-ergodic dynamics (Fig. 2). In order to inhibit gelation effects, the sample was diluted to 0.5 wt.% AAKLVFF, which resulted in the suppression of the 'gelation' peak, as can be observed in Fig. 2.

DLS has already been used to study the formation of amyloid fibres from many peptides and fibrils, such as β-lactoglobulin [8–10]. The

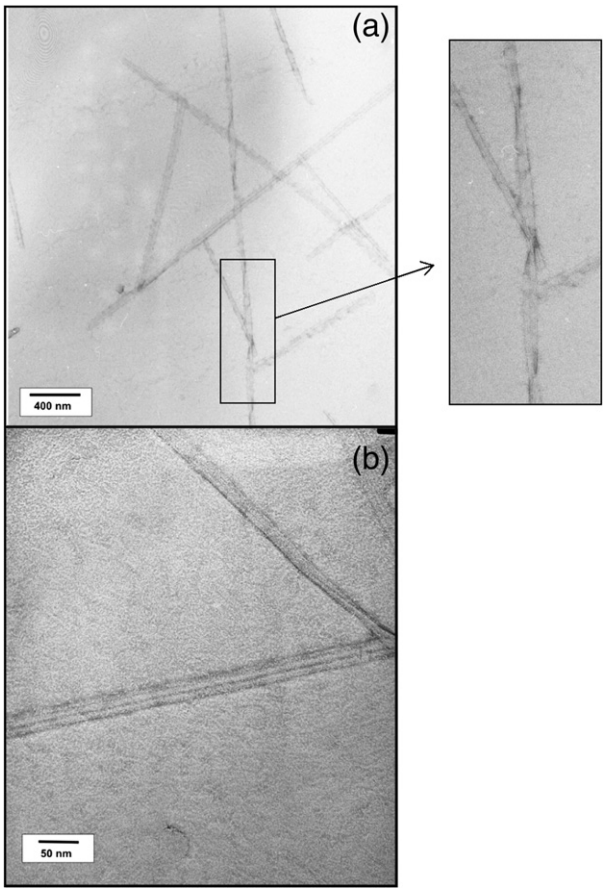

Fig. 1. (a) TEM and (b) HR-TEM images of fibrils formed by 1 wt.% AAKLVFF in water.

field correlation function from a solution of protein fibres several tens of nanometers in length presents a single exponential behaviour, corresponding to a single relaxation mode with a well-defined hydrodynamic radius. We found that it was necessary to account for a distribution of relaxation times in analysing DLS data from AAKLVFF. A stretched exponential function to model $g^{(1)}(q,t)$ allows for a spectrum of relaxation times resulting from the internal modes of the fibres:

$$g^{(1)}(q,t) = A_0 + A_1 \exp\left(-\left[t/\tau_\beta\right]^\beta\right) \quad (3)$$

Here τ_β is a characteristic decay time of the system, A_i are the relative scattering amplitudes of the system and the exponent β ($0 \le \beta \le 1$) is a measure of the width of the corresponding distribution of relaxation times, the smaller the value of β, the broader is the distribution. The mean characteristic time, $\bar{\tau}_\beta$, of the stretched exponential mode is given by $\bar{\tau}_\beta = (\tau_\beta/\beta)\Gamma(1/\beta)$ where $\Gamma(1/\beta)$ is the gamma function. The corresponding decay rate is $\bar{\Gamma}_\beta = 1/\bar{\tau}_\beta$. An alternative procedure to describe a distribution of decay rate is the method of cumulants, as used for example by Murphy and co-workers to analyse DLS data from amyloid β (Aβ) peptide fragments [2,11,12]. Here, we have used the alternative, Eq. (3).

DLS curves measured in the interval $50 \le \theta \le 150°$ were used to calculate the corresponding $g^{(1)}(q,t)$ Eq. (2). The resulting field correlation function was then fitted to Eq. (3). The parameter β was fixed to 0.75 for all the fittings which is the value expected for a system of semi-flexible polymers ($\beta = 3/4$) [13]. Fig. 3a shows a representative example for $g^{(1)}(q,t)$ calculated for $\theta = 70°$, while Fig. 3b shows the dependence of $\bar{\Gamma}_\beta$ with q^2 obtained from the fitting of the correlation functions using Eq. (3).

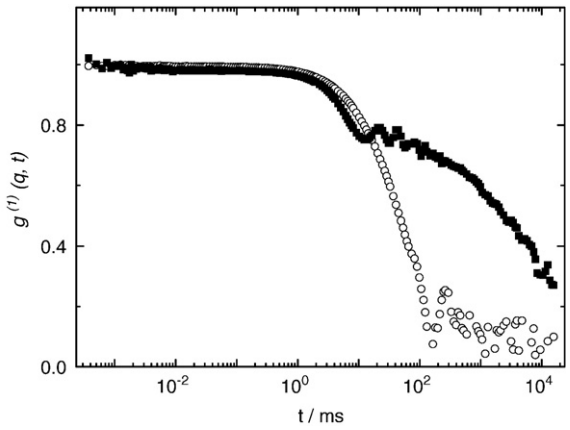

Fig. 2. Field correlation function calculated for (■) 1 and (○) 0.5 wt.% AAKLVFF in water. The correlation functions have been arbitrarily normalized to a common scale in order to enable the visualization of the data.

The straight line for the q^2 dependence of $\bar{\Gamma}_\beta$ in Fig. 3b does not pass through the origin, suggesting that $\bar{\Gamma}_\beta$ should be associated to an internal mode of the AAKLVFF fibrils.

If a system presents diffusive dynamics, the decay rate approaches zero at $q=0$. The diffusion coefficient D can then be calculated from the gradient of the plot of Γ vs. q^2 according to the expression:

$$\bar{\Gamma}_\beta = Dq^2 \quad (4)$$

But, since the straight line for the q^2 dependence of $\bar{\Gamma}_\beta$ in Fig. 3b does not pass through the origin, Eq. (4) had to be modified to include an

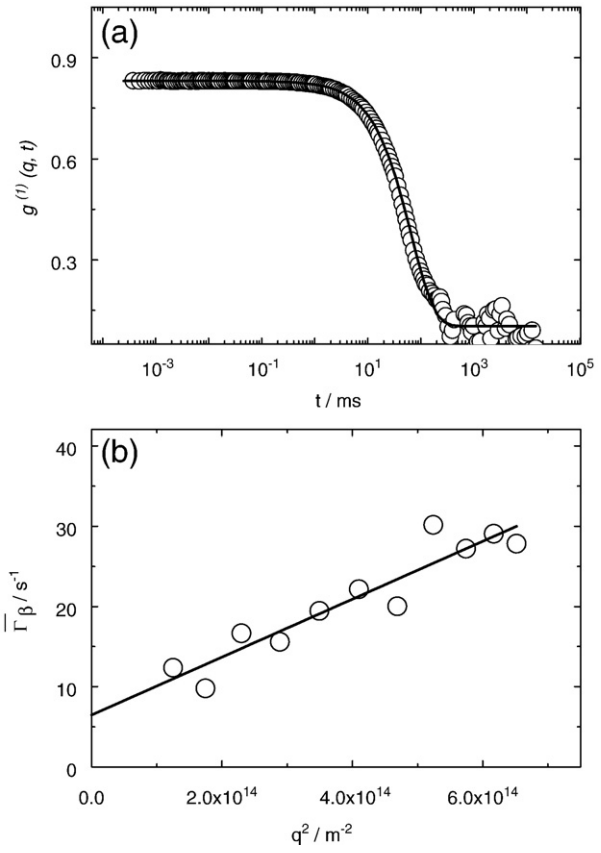

Fig. 3. DLS results for 1 wt.% AAKLVFF: (a) Field correlation function for 70°, fitted according to Eq. (3), and (b) variation of $\bar{\Gamma}_\beta$ with q^2, obtained from the fitting of the DLS data using Eq. (3).

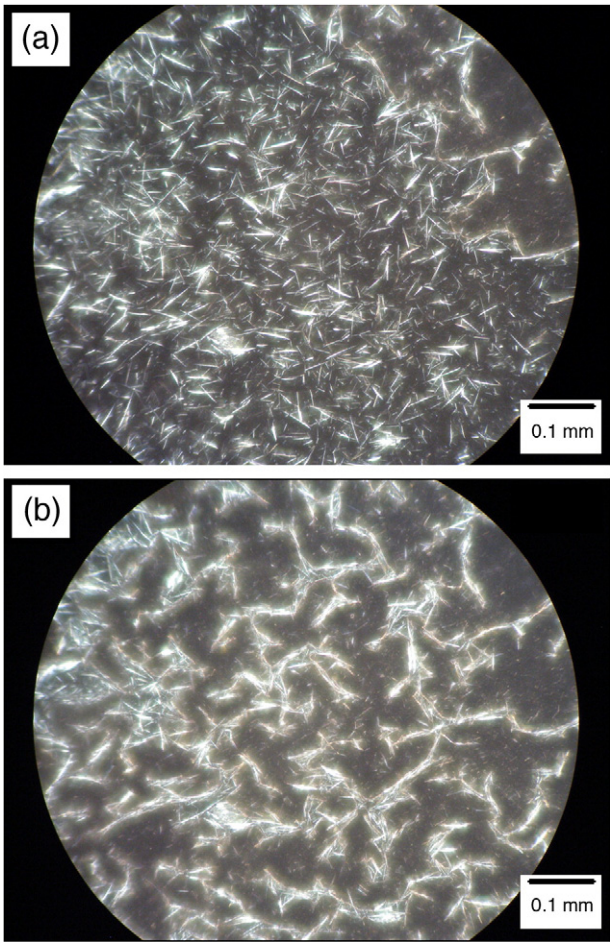

Fig. 4. POM images of AAKLVFF crystals obtained at (a) t=0 s and (b) t=5 s after the sample has spontaneously started to dry. Photos (a) and (b) have been taken over the same area of the sample.

additional constant offset. However, it is possible to base the analysis of the dynamics defining D_f as the gradient of the line excluding the constant offset, which will be understood as an "effective diffusion coefficient". In this way, it is possible to calculate from the slope in Fig. 3a a value $D_f = 3.6\times10^{-14}$ m^2 s^{-1}.

Since the diffusion coefficient and the hydrodynamic radius are reciprocally related by the Stokes–Einstein equation, and this D_f value is smaller than $D = 3.8\times10^{-13}$ m^2 s^{-1} reported for AAKLVFF nanotubes in methanol [6], the AAKLVFF fibrils in water occupy a larger volume than the nanotubes in methanol.

The ageing of AAKLVFF fibrils was investigated by microscopy. A small volume (1 ml) of 1 wt.% AAKLVFF solution was matured for 5 days in a glass vial. Observation by naked eyes of the matured sample revealed phase separation into two phases, consisting of a solid white precipitate of peptide on the bottom of the vial and a top layer of aqueous solution which may contain AAKLVFF aggregates. This result shows that the white precipitate of peptide is heavier than water and probably consists of AAKLVFF crystals or hydrated fibrillar aggregates. The crystallization of peptides upon incubation in an aqueous phase has already been noted, for example for KFFEAAAKKFFE which crystallized after incubation of the peptide for several days in a phosphate buffer saline (PBS) aqueous solution [14]. Needle-shape crystals were observed, with lengths in the order of micrometers and diameters in the range ~(12–240) nm [14].

The partially hydrated AAKLVFF precipitate of the 1 wt.% peptide matured sample was studied by POM. Fig. 4a shows a POM image obtained for the precipitate placed between a glass slide and a coverslip, at time t=0 s. Fig. 4b shows a photograph of the same area taken at t=5 s, after the spontaneous process of drying the partially hydrated precipitate under the coverslip has started. A qualitative evaluation of the results in Fig. 4 reveals that the incubation of AAKLVFF in water gives rise to needle-shape crystals with an average length of (41.2±9.4) μm and an average width of (2.4±0.8) μm. These are much larger than the dimensions of the fibrous crystals observed for KFFEAAAKKFFE, suggesting a higher crystallization propensity in AAKLVFF. It is probable that the change in configuration between Fig. 4a and b results from further crystallization upon drying.

3.2. Secondary structure of AAKLVFF fibrils

The secondary structure of the AAKLVFF fibrils observed in a 1 wt.% peptide solution, was studied for dried films, using FT-IR in transmission and grazing incidence modes. The FT-IR spectra in transmission and grazing incidence mode obtained in the wavenumber ranges of (1350–1975) cm^{-1} and (2500–3825) cm^{-1} are shown in Fig. 5a and b respectively. The direct comparison of transmission and grazing incidence FT-IR results has already been used by Hartgerink and co-workers [15] as a strategy to determine the orientation of the β-sheets with respect to the main axis of the fibril, in β-sheet nanofibers of peptide-amphiphiles.

The orientation of the sample surface is perpendicular to the incident IR beam for the transmission FT-IR experiments, while for grazing incidence FT-IR experiments the beam is almost parallel to the surface of the sample. As already pointed out by Hartgerink and co-workers [15] peptide fibrils with a large length-to-diameter radius will lie flat when deposited as a dry film onto a solid surface. This

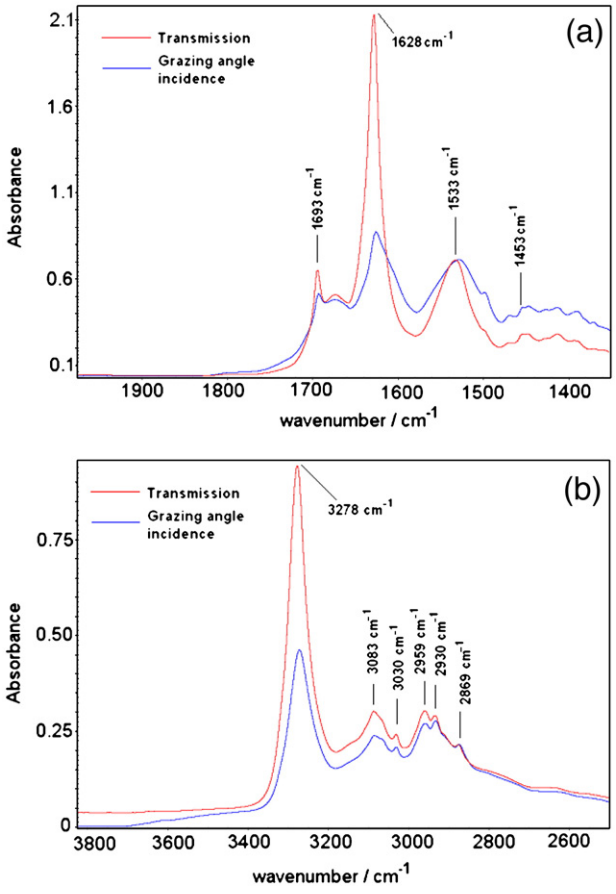

Fig. 5. FT-IR spectra in the (red line) transmission and (blue line) grazing incidence configurations obtained for a dried film of 1 wt.% AAKLVFF in water, obtained for (a) 1350–1975 cm^{-1} and (b) 2500–3825 cm^{-1}.

applies to AAKLVFF fibrils, which have a large length to diameter ratio (according to TEM, length/radius>5000 nm/30 nm). Therefore, a change in the angle between the IR beam and the sample surface is equivalent to a change in the angle between the IR beam and the amide bond.

Fig. 5 shows that both the grazing incidence and transmission FT-IR data present absorbance peaks at similar wavenumbers but with different intensity.

FT-IR spectra in the amide I band are sensitive to secondary structure (Fig. 5a). The peaks at 1693 and 1628 cm^{-1}, in the amide I band, are associated with a β-sheet structure [16,17]. In particular, the strong amide I band at 1628 cm^{-1} in combination with the weaker amide I band at 1693 cm^{-1} obtained for the transmission FT-IR, suggests an antiparallel β-sheet conformation of the peptide chains [16–18].

The peak at 1453 cm^{-1} is associated with the amide II band [17,19], while the peak at 1533 cm^{-1} is associated with the N–H in-plane bending or C–N stretching modes [20].

Additional FT-IR peaks were located in the amide A band at 3278 cm^{-1} and amide B band at 3083 cm^{-1} (Fig. 5b). An absorption peak at 3030 cm^{-1} was due to the stretching vibration from the benzene rings. A peak at 2959 cm^{-1} was due to the CH_3 vibration. A peak at 2930 cm^{-1} was assigned to the CH_2 asymmetric stretching bands while a peak at 2869 cm^{-1} was due to the CH_3 symmetric stretching bands.

Fig. 5a provides evidence of β-sheet structure in the AAKLVFF fibrils in the dried film. The results in Fig. 5a show that the amide I band is attenuated and the amide II band is enhanced in the grazing incidence configuration. Hartgerink and co-workers [15] show that this occurs when the IR laser beam is oriented parallel to the C=O bonds. These are oriented along the fibril axis. This alone does not enable twisted fibrils to be differentiated from untwisted ones, however the TEM clearly shows the twisted structure.

In a previous work we showed that AAKLVFF self-assembles in methanol into nanotubes. It was suggested that the walls of the nanotubes arise from the helical wrapping of AAKLVFF β-sheets [6]. The fibril model for AAKLVFF in water (represented by β-strands twisted around a common axis) is consistent with that previously proposed by us for the structure of AAKLVFF nanotubes in methanol [6], but here the β-sheets do not close into nanotubes, possibly due to unfavourable interactions between ribbon edges. Both models for the AAKLVFFF nanotube or fibril follow the geometrical relationships for winding of a tape into a helical ribbon developed by Chung et al. [21]. The tendency for the β-sheets to twist into ribbons [22] results from the interfacial curvature with its origin in the packing of side

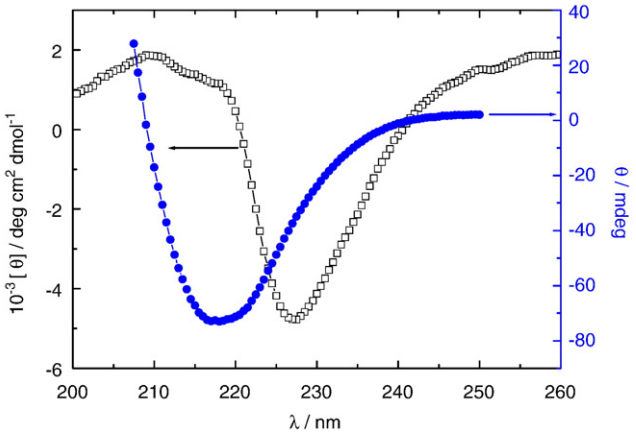

Fig. 6. CD spectrum of 1 wt.% AAKLVFF in water and for a dried film. For the dried film, it is not possible to convert to units of molar ellipticity since the concentration is not defined and film thickness (pathlength) is not known.

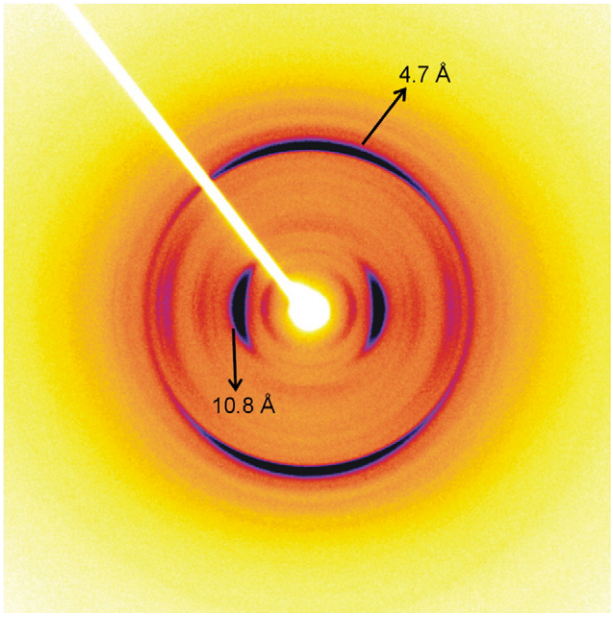

Fig. 7. X-ray diffraction pattern from a peptide dried stalk prepared using a 1 wt.% AAKLVFF solution. The tilted white line is the beamstop.

chains with different effective volumes (e.g. aromatic vs. non-aromatic residues).

SAXS shows that AAKLVFF nanotubes in methanol have a diameter of (72±8) nm [6], which is similar to the (63±18) nm diameter measured in this work using HR-TEM for the AAKLVFF fibrils in water (when dried, TEM suggested that the AAKLVFF nanotubes unwrap to give 130 nm wide sheets). This suggests that the nanotubes are "fully wrapped" ribbons, as suggested in our original work. The formation of closed nanotubes may result from changes in solution permittivity in methanol compared to water. This may modulate the electrostatic interactions between ribbon edges resulting from the charged peptide termini and lysine residue, which may lead to closed nanotube formation. An alternative explanation is based on differences in β-strand registry in fibrils compared to nanotubes. Strands may be staggered in the nanotubes. It may be noted that the β-sheet width may also differ in methanol compared to water due to different H-bond strengths.

CD experiments were undertaken on a 1 wt.% AAKLVFF solution and on a dried film obtained from a 0.5 wt.% AAKLVFF solution, to provide additional information on the secondary structure of the fibril. Fig. 6 shows the CD spectra obtained for the AAKLVFF solution and dried film. The spectrum for the dried film is dominated by a negative maximum at 217 nm, which denotes a β-sheet structure [23]. In contrast, the CD spectrum for the solution contains a red-shifted negative maximum at 228 nm and a positive band at 209 nm. Such spectra are often ascribed to β-turn structures [23–25]. We can alternatively interpret the CD spectrum from the solution on the basis

Table 1
Observed and calculated *d* spacings, calculated for the indexation of the XRD pattern in Fig. 7

Miller indices [*hkl*]	Predicted position [Å]	Measured position [Å] ±0.1
011	17.12	17.01
004	10.94	10.84
021	9.10	9.03
015	7.92	7.98
024	7.09	7.11
008	5.47	5.46
027	5.19	5.19
100	4.82	4.81

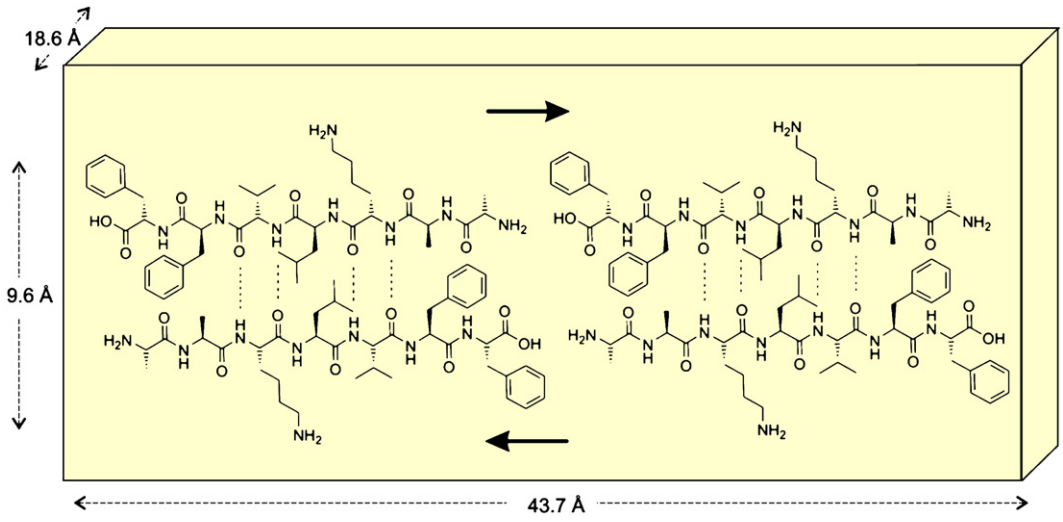

Scheme 2. Model for the packing of AAKLVFF antiparallel β-sheets in an orthorhombic cubic cell. The dimensions of the unit cell are taken from XRD results while the (antiparallel) packing of the β-sheets agrees with FT-IR data.

that the positive maximum due to n–π* aromatic stacking interactions between phenylalanine residues in solution [4,5] causes a red-shift of the negative maximum at 217 nm.

XRD was used to provide further evidence of amyloid fibril formation in a dried film, and to gain an insight into their secondary structure. Stalks of peptide were prepared by drying a thread of 1 wt.% AAKLVFF solution between the ends of two waxed capillaries. The sample was partially aligned by stretching the thread before the drying process started, and the resulting XRD pattern (Fig. 7) shows a well-defined "cross-β" pattern [1] with, unusually for amyloid fibrils, multiple orders of reflection. This facilitates determination of the unit cell, which was performed using the software CLEARER [14]. The results provided an orthorhombic unit cell, with unit axis a=9.6 Å, b=18.6 Å and c=43.7 Å. The values of the observed and calculated reflections corresponding to the indexation of the XRD pattern in Fig. 7, is shown in Table 1. It is possible to understand the values of the orthorhombic unit cell parameters in terms of the AAKLVFF packing within the β-sheet. Within that frame, the cell axis a represents the peptide backbone separation within a β-strand [4] while the cell axis b corresponds to the spacing of two β-sheets (with relatively small side groups, and efficient packing) [4]. Assuming that all the peptide residues are in the β-sheet, the cell axis c corresponds to two AAKLVFF molecules (each AAKLVFF molecule is 7×3.4=23.8 Å long assuming a 7 residue antiparallel β-sheet). Scheme 2 shows the packing of the AAKLVFF β-strand within the unit cell, according to the indexation of the XRD data in Fig. 7. The peptide β-sheet results from the repetition in space of the unit cell in Scheme 2, with a twist around a central axis, according to the model for the peptide fibril discussed above in relation to FT-IR results. The dimensions of the orthorhombic cell determined for AAKLVFF fibrils are very similar to those reported in the literature for fibrils of KFFEAAAKKFFE, i.e., a=9.5 Å, b=21.3 Å and c=48.1 Å [14]. The c axis in this case is larger than for AAKLVFF, consist with the greater length of the 12 residue peptide.

According to XRD results, the thickness of two β-sheets of AAKLVFF is ~18.6 Å. TEM and HR-TEM show that the average width of an AAKLVFF fibril is (63±18) nm, and that each fibre is made of three (21±6) nm wide protofilaments. The thickness of the ribbons is approximately ten times lower than its width (Fig. 1). It appears that the fibrils observed in TEM are higher order aggregates of tape-like protofilaments, containing multiple repeats of the unit cell b and c axes orthogonal to the fibril (a) axis. It would seem likely that the β-sheets are arranged in a flat configuration with hydrophobic residues (especially phenylalanine) on one face and in the interior of the individual tapes and that the b axis is associated with the ribbon thickness, although this is not unambiguous.

4. Summary

The self-assembly of AAKLVFF in water has been investigated. This study builds on our previous work on AAKLVFF in methanol solutions, for which nanotube formation is observed [6]. It is remarkable that only the substitution of the methanol by water is enough to give rise to a distinct motif, i.e. peptide fibrils which are observed for dried films. It appears that in more dilute aqueous solutions, AAKLVFF may not form well-defined β-sheet structures as revealed by circular dichroism. This is similar to our findings for KLVFF [4]. The AAKLVFF peptide fibrils are quite clearly resolved by TEM and HR-TEM, which suggest a twisted tape-like fibril structure, while their semi-flexible nature is revealed by DLS. FT-IR shows that AAKLVFF forms β-sheets in dried films, as does CD. However, the latter technique indicates that AAKLVFF does not form well-defined β-sheets in dilute solution. Our model for the peptide fibril structure agrees with the structure of AAKLVFF nanotubes in methanol, where the β-strands are also twisted along a common main axis but are staggered, giving rise to the formation of a nanotube (i.e. with a hollow core around the common main axis) formation. FT-IR and CD results were supported by XRD data, which provided additional evidence for the packing of AAKLVFF into β-strands in dried films.

AAKLVFF forms very well defined fibrils, assembled from smaller sub-units in films dried from aqueous solutions and may be a model system for further studies in amyloid fibrillisation.

Acknowledgements

We thank Dr. Rebecca Green (Dept of Pharmacy, University of Reading) for access to the FT-IR instrument, Dr. Louise C. Serpell (Dept. of Biochemistry, Univ. of Sussex) for providing a copy of the software CLEARER and Mr. Nick Spencer (Biocentre, Univ. of Reading) for assistance with XRD experiments.

References

[1] I.W. Hamley, Peptide fibrillization, Angew. Chem. (Int. Ed.) 46 (2007) 8128–8147.
[2] C.-L. Shen, M.C. Fitzgerald, R.M. Murphy, Effect of acid predissolution on fibril size and fibril flexibility of synthetic β-amyloid peptide, Biophys. J. 67 (1994) 1238–1246.

[3] C. Soto, E.M. Sigurdsson, L. Morelli, R.A. Kumar, E.M. Castaño, B. Frangione, β-sheet breaker peptides inhibit fibrillogenesis in a rat brain model of amyloidosis: implications for Alzheimer's therapy, Nat. Med. 4 (1998) 822–826.
[4] M.J. Krysmann, V. Castelletto, A. Kelarakis, I.W. Hamley, R.A. Hule, D.J. Pochan, Self-assembly and hydrogelation of an amyloid peptide fragment, Biochemistry 47 (2008) 4597–4605.
[5] M.J. Krysmann, V. Castelletto, I.W. Hamley, Fibrillisation of hydrophobically modified amyloid peptide fragments in an organic solvent, Soft Matter 2 (2007) 1401–1406.
[6] M.J. Krysmann, V. Castelletto, J.E. McKendrick, L.A. Clifton, I.W. Hamley, P.J.F. Harris, S.M. King, Self-assembly of peptide nanotubes in an organic solvent, Langmuir 24 (2008) 8158–8162.
[7] B.J. Berne, R. Pecora, Dynamic Light Scattering, Wiley-Interscience, New York, 1976.
[8] P. Aymard, T. Nicolai, D. Durand, Static and dynamic scattering of beta-lactoglobulin aggregates formed after heat-induced denaturation at pH 2, Macromolecules 32 (1999) 2542–2552.
[9] L.N. Arnaudov, R. de Vries, H. Ippel, C.P.M. Van Mierlo, Multiple steps during the formation of β-lactoglobulin fibrils, Biomacromolecules 4 (2003) 1614–1622.
[10] V. Castelletto, I.W. Hamley, b-lactoglobulin fibers under capillary flow, Biomacromolecules 8 (2007) 77–83.
[11] C.-L. Shen, R.M. Murphy, Solvent effects on self-assembly of β-amyloid peptide, Biophys. J. 69 (1995) 640–651.
[12] C.-L. Shen, G.L. Scott, F. Merchant, R.M. Murphy, Light scattering analysis of fibril growth from amino-terminal fragment b(1–28) of β-amyloid peptide, Biophys. J. 65 (1993) 2383–2395.
[13] K. Kroy, E. Frey, Dynamic scattering from solutions of semiflexible polymers, Phys. Rev. E 55 (1997) 3092–3101.
[14] O.S. Makin, E. Atkins, P. Sikorski, J. Johansson, L.C. Serpell, Molecular basis for amyloid fibril formation and stability, Proc. Nat. Acad. Sci. (USA) 102 (2005) 315–320.
[15] S.E. Paramonov, H.W. Jun, J.D. Hartgerink, Self-assembly of peptide-amphiphile nanofibers: the roles of hydrogen bonding and amphiphilic packing, J. Am. Chem. Soc. 128 (2006) 7291–7298.
[16] P. Haris, D. Chapman, The conformational analysis of peptide using Fourier Transform IR spectroscopy, Biopolymers 37 (1995) 251–263.
[17] B. Stuart, Biological Applications of Infrared Spectroscopy, Wiley, Chichester, 1997.
[18] T. Miyazawa, E.R. Blout, The infrared spectra of polypeptides in various conformations: amide I and II bands, J. Am. Chem. Soc. 83 (1961) 712–719.
[19] S.-Y. Lin, H.-L. Chu, Fourier transform infrared spectroscopy used to evidence the prevention of β sheet formation of amyloid β(1–40) peptide by short amyloid fragment, Int. J. Biol. Macromol. 32 (2003) 173–177.
[20] S. Sarkar, A. Chourasia, S. Maji, S. Sadhukran, S. Kumar, B. Adhikari, Synthesis and characterization of gelatin based polyester urethane scaffold, Bull. Mat. Sci. 29 (2006) 475–484.
[21] D.S. Chung, G.B. Benedek, F.M. Konikoff, J.M. Donovan, Elastic free energy of anisotropic helical ribbons as metastable intermediates in the crystallization of cholesterol, Proc. Nat. Acad. Sci. (USA) 90 (1993) 11341–11345.
[22] I.A. Nyrkova, A.N. Semenov, A. Aggeli, M. Bell, N. Boden, T.C.B. McLeish, Fibril stability in solutions of twisted β-sheet peptides: a new kind of micellization in chiral systems, Eur. Phys. J. B 17 (2000) 499–513.
[23] S.M. Kelly, T.J. Jess, N.C. Price, How to study proteins by circular dichroism, Biochim. Biophys. Acta 1751 (2005) 119–139.
[24] P.-Y. Cheng, β-Forming protein chain in a globular enzyme, deoxyribonuclease I*, Proc. Nat. Acad. Sci. (USA) 55 (1966) 1535–1538.
[25] E.R. Blout, E. Schechter, A new technique for producing oriented synthetic polypeptides: Some initial results, Biopolymers 1 (1963) 565.